PLANETARY SCIENCE

Zhurong reveals recent aqueous activities in Utopia Planitia, Mars

Yang Liu[1,2]*, Xing Wu[1], Yu-Yan Sara Zhao[3,2], Lu Pan[4], Chi Wang[1], Jia Liu[1], Zhenxing Zhao[1,5], Xiang Zhou[1,5], Chaolin Zhang[1,5], Yuchun Wu[1,5], Wenhui Wan[6], Yongliao Zou[1]

The Mars' climate is cold and dry in the most recent epoch, and liquid water activities are considered extremely limited. Previous orbital data only show sporadic hydrous minerals in the northern lowlands of Mars excavated by large impacts. Using the short-wave infrared spectral data obtained by the Zhurong rover of China's Tianwen-1 mission, which landed in southern Utopia Planitia on Mars, we identify hydrated sulfate/silica materials on the Amazonian terrain at the landing site. These hydrated minerals are associated with bright-toned rocks, interpreted to be duricrust developed locally. The lithified duricrusts suggest that formation with substantial liquid water originates by either groundwater rising or subsurface ice melting. In situ evidence for aqueous activities identified at Zhurong's landing site indicates a more active Amazonian hydrosphere for Mars than previously thought.

INTRODUCTION

Although ancient Mars has long been hypothesized to be wet and habitable, the most recent epoch of Mars geologic history, Amazonian, is often considered cold and dry. Like the surface conditions of modern Mars, water activities during the Amazonian primarily included deposition and erosion of the polar ice caps, while the occurrence of liquid water was limited (*1*). The correlation of the widespread occurrence of hydrated minerals in the ancient southern highlands and their absence in the Amazonian surfaces of northern lowlands support this view from the mineralogical perspective (*2*). Various ice-dominated landforms within the midlatitude, including concentric crater fill, linear valley fill, and terraced craters, allude to common icy conditions in the Amazonian age (*3*–*5*). However, recent analyses have identified fluvial geomorphology crosscutting the Amazonian-aged terrains (e.g., within Lyot crater) (*6*–*8*), suggesting that the recent epoch of Mars could have been more active with liquid water sculpting the surface. Although northern lowlands surface units may have formed via episodic flooding and ice deposition events in the Amazonian (*9*), the timing, duration, and nature of water activities during this epoch remain open questions. With northern lowlands largely covered by dust that obscures spectroscopic signatures from the orbits, only sporadic hydrous minerals were identified mainly within large impact craters, interpreted as excavated ancient strata (*10*, *11*). Some hydrated mineral (including hydrated silica) signatures associated with cones and flow features have also been identified in the northern plains, but only in localized areas due to limited coverage of the orbital data [e.g., (*12*)]. Therefore, in situ geochemical and mineralogical investigations on Amazonian-aged geologic units are imperative to constrain the types, characteristics, and duration of potential aqueous activities in the recent epoch of Mars.

The Tianwen-1 Mars mission successfully landed the Zhurong rover in the southern Utopia Planitia at 25.066°N, 109.925°E (Fig. 1) (*13*). The Utopia Planitia is the largest recognized impact basin in the northern lowlands of Mars (*14*), and it was flooded and filled by the Hesperian-aged Vastitas Borealis Formation materials (*15*). Many morphological features (i.e., pitted cones, giant polygons, ghost craters, and layered ejecta craters) have led to the hypothesis that the surface layer contains a substantial amount of volatiles (*16*). The landing area of Zhurong has been carefully characterized using orbital data before and shortly after the landing (*13*, *17*–*21*). These studies show that the landing area has been resurfaced around the middle Amazonian (*18*), and the materials on the current terrain could be as young as ~700 Ma from crater counting statistics (*21*). Various geological features, including pitted cones, ghost craters, mesas, troughs, and ridges, occur within 30 km of the Zhurong rover touchdown site (Fig. 1A), indicative of possible volatile presence in the shallow subsurface. However, previous orbital investigations did not find any hydrated minerals in the vicinity of the landing area (*18*), partially due to the limited coverage of the orbital observations with high spatial resolution, casting doubts on the formation mechanism of such landforms and the nature of water activities in this region.

Equipped with six scientific payloads (fig. S1), the main objectives of the Zhurong rover are to investigate the morphology, mineralogy, space environment, subsurface structure, and water/ice distribution of the southern Utopia Planitia (*22*, *23*). Until 4 September 2021, the Zhurong rover has completed its nominal exploration period for 92 sols and returned valuable scientific data collected along its traverse. In particular, the Mars Surface Composition Detector (MarSCoDe) (*24*) and Navigation and Terrain Camera (NaTeCam) (*25*) onboard the rover provide an unprecedented opportunity to characterize the morphology of the landing area and compositions of the surface materials. Here, we report the preliminary results of the mineralogy and sedimentary characteristics and their implications for the geological and climate evolution in the Utopia basin.

RESULTS

The terrain Zhurong traverse is smooth with a few rocks and resolvable granules and pebbles (Fig. 2 and fig. S2), mainly composed of

[1]State Key Laboratory of Space Weather, National Space Science Center, Chinese Academy of Sciences, Beijing 100190, China. [2]Center for Excellence in Comparative Planetology, Chinese Academy of Sciences, Hefei 200083, China. [3]Center for Lunar and Planetary Sciences, Institute of Geochemistry, Chinese Academy of Sciences, Guiyang 550081, China. [4]Center for Star and Planet Formation, GLOBE Institute, University of Copenhagen, Copenhagen, Denmark. [5]University of Chinese Academy of Sciences, Beijing 100049, China. [6]State Key Laboratory of Remote Sensing Science, Aerospace Information Research Institute, Chinese Academy of Sciences, Beijing 100101, China.
*Corresponding author. Email: yangliu@nssc.ac.cn

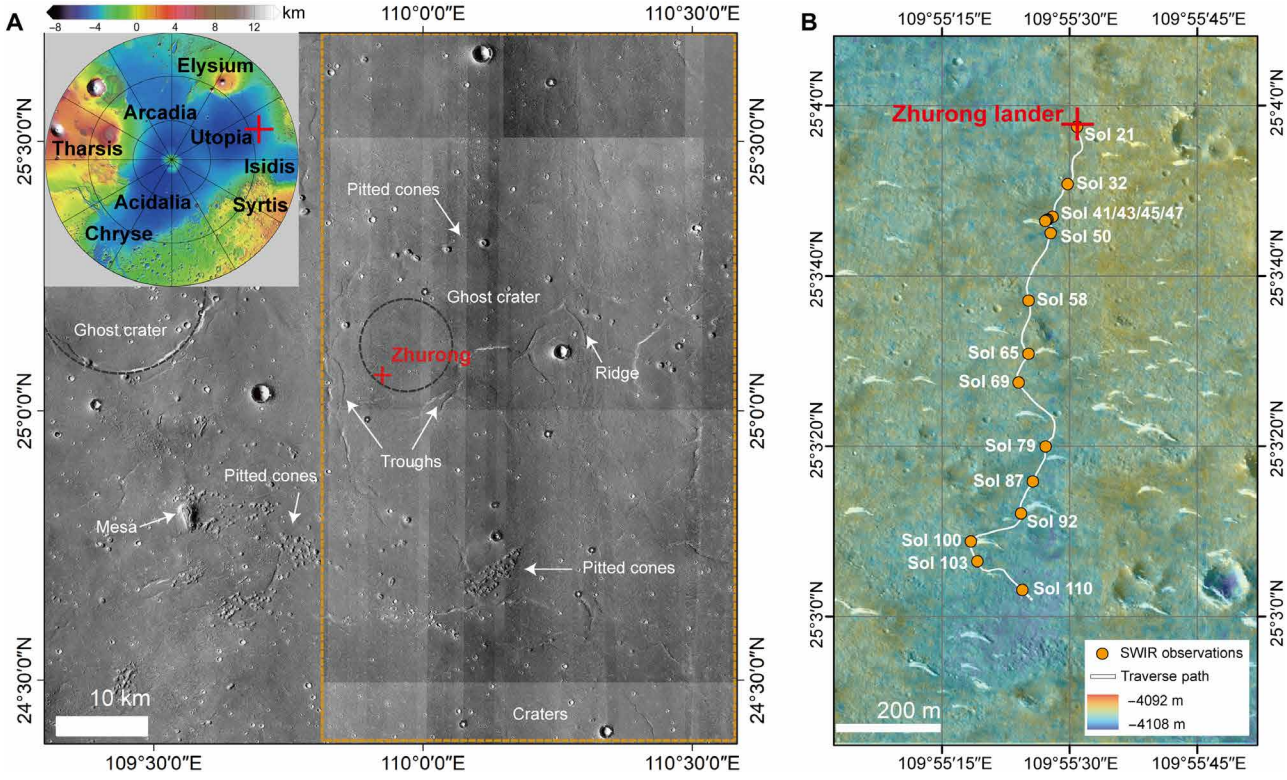

Fig. 1. Geologic context of Zhurong landing site. (**A**) The inset Mars Orbiter Laser Altimeter (*49*) topographic map displays the Northern Hemisphere of Mars. The Zhurong rover (red cross) is located in the southern Utopia Planitia. Tianwen-1 High Resolution Imaging Camera (HiRIC; ~0.7 m per pixel) (*50*) image (outlined by orange dashed lines) overlays the Mars Reconnaissance Orbiter Context Camera (~6 m per pixel) (*51*) image showing the diverse geomorphological features of the landing site, denoted by arrows. (**B**) The traverse of Zhurong rover is denoted by the white line. The orange dots indicate spots of spectral observations. The basemap is a HiRIC image overlain by the HiRIC digital terrain model (~3.5 m per pixel).

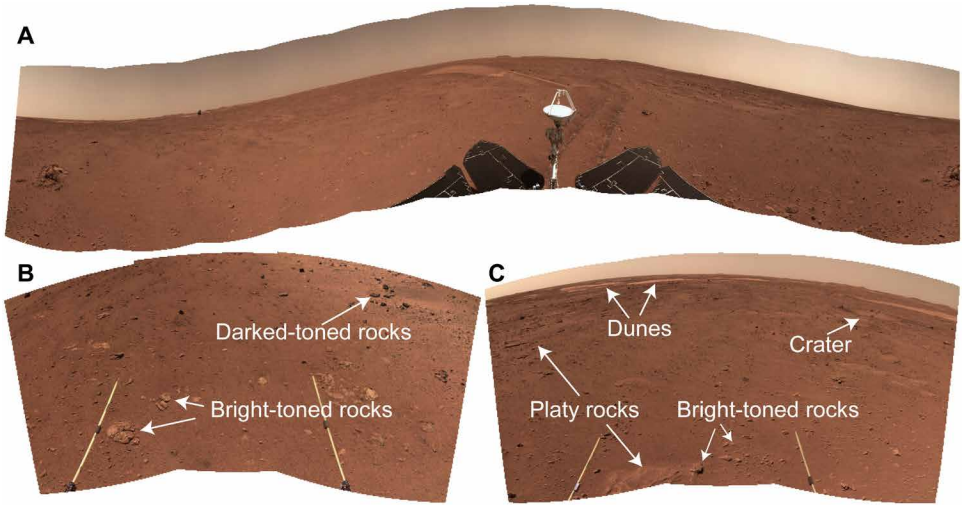

Fig. 2. The local context of the terrain Zhurong traverse. (**A**) The NaTeCam panorama on sol 50 displays the landing area and its immediate surroundings. (**B**) A close-up image taken on sol 22 shows the dark-toned and bright-toned rocks, which are two primary rocks distributed in this region (also see fig. S2). (**C**) Image taken on sol 57 displays platy rocks, bright-toned rocks, dunes, and a small crater.

sand-sized particles ranging between 500 μm and 2 mm consistent with the thermal inertia values of 250 to 350 J K^{-1} m^{-2} $s^{-1/2}$ (*18*, *21*, *26*). Clustered, embedded, and buried rocks are all observed modulated by the impact process and the removal or deposition of fine-grained sands (fig. S2B). Two distinct types of rocks were observed (Fig. 2B and fig. S3). One dark-toned rock group often is exposed in the far field (Fig. 2B), with predominantly angular shapes and varying sizes. Some of these dark-toned rocks show vesicular

surfaces (fig. S3C). Because the dark-toned rocks often distribute on the rim of small buried impact craters, they are interpreted as excavated basaltic rocks. On the other hand, bright-toned rocks in the NaTeCam images, ranging from 8 to 18 cm in size, are scattered on the ground in clustered patches (Fig. 2, B and C). These rocks often are covered by dust and soils and show flaking or peeling surfaces, suggesting physical weathering by thermal stress and aeolian processes (Fig. 3). Some of these bright rocks (Fig. 3, sol 45) with light-toned rinds have dark interiors that is distinctive from these flaking rocks (Fig. 3, sols 32 and 43). We identify several small, simple craters surrounded by ejected fragments and sometimes entirely buried by fines (fig. S2B). Aeolian bedforms (e.g., dunes or ripples) are common in the landing areas, covered by both bright and dark sands on the surface (fig. S2C).

The bright-toned rocks were targeted by the MarSCoDe shortwave infrared (SWIR) spectrometer that acquires radiance spectra between 0.8 and 2.4 μm in 321 channels with a field of view (FOV) of 36.5 mrads. After conversion to reflectance (see Materials and Methods), we identified a distinct spectral class of hydrated minerals using the spectra over a few bright-toned rocks (sols 32, 43-1, 43-2, and 45), which has not been identified previously using orbital data (Fig. 3). For example, analysis of the data from the Observatoire pour la Minéralogie, l'Eau, les Glaces, et l'Activité (OMEGA) (*2*) onboard Mars Express covering the landing area shows no hydration features. These spectra have a distinct asymmetric 1.93- to 1.95-μm absorption feature, attributed to the combination mode of structural H_2O (Fig. 3). A relatively weak absorption at 1.45 μm may be present. Most spectra show an additional absorption around 2.22 μm, except for the rock measured on sol 45 interpreted to be a basaltic rock. This rock on sol 45 has large angular grains (2 to 3 cm) and appears bulkier and less weathered than its counterparts, with a dark-toned interior inside the light-toned rinds on the surface. The spectra of a few targets, including other bright-toned platy rocks and basaltic rocks, are shown in fig. S4. The spectral ratio between hydrated targets and targets that lack hydrated minerals shows that the bright-toned rocks exhibit both 1.9- and 2.2-μm features despite the low signal-to-noise ratio of the ratio spectra (fig. S4). The asymmetric ~1.9-μm absorption feature is common among hydrated minerals with structural H_2O. The ~2.2-μm absorption feature is diagnostic of hydroxyl stretching in silica, aluminum clay, or hydrated sulfate. Al-phyllosilicates (such as montmorillonite) have an absorption feature at ~2.2 μm, but the band is narrower and shift to short wavelengths compared to that in the MarSCoDe spectra. The ~2.2-μm absorption of the bright-toned rocks has a width spreading from 2.13 to 2.30 μm (Fig. 3), most consistent with hydrated silica (*27*). Gypsum has multiple absorptions between 2.21 and 2.27 μm (*28*). When mixed with other phases, the ~2.2-μm triplet of gypsum is less well defined, providing a potential spectral match for the MarSCoDe spectra (*29*). The band center of the 1.9-μm feature in the MarSCoDe SWIR spectra is shifted to a longer wavelength (1.93 to 1.95 μm) compared to typical opaline silica (1.91 μm), with the exception of opal-CT formed under hydrothermal conditions (*30*). Alternatively, the 1.9-μm feature could be explained by hydrated sulfates including gypsum, bassanite, and epsomite (fig. S5). At present, the observed major spectral features could be explained by hydrated silica or hydrated sulfates. However, the low signal-to-noise ratio and the absence of other diagnostic features preclude an unambiguous mineral identification. With more spectral data acquired by the rover in the future, examining correlations between 1.9- and 2.2-μm absorption features in different types of geological targets may help test current interpretations.

From sol 24 onward, the Zhurong rover has continuously observed planar rock flats, some in perched position and slightly above

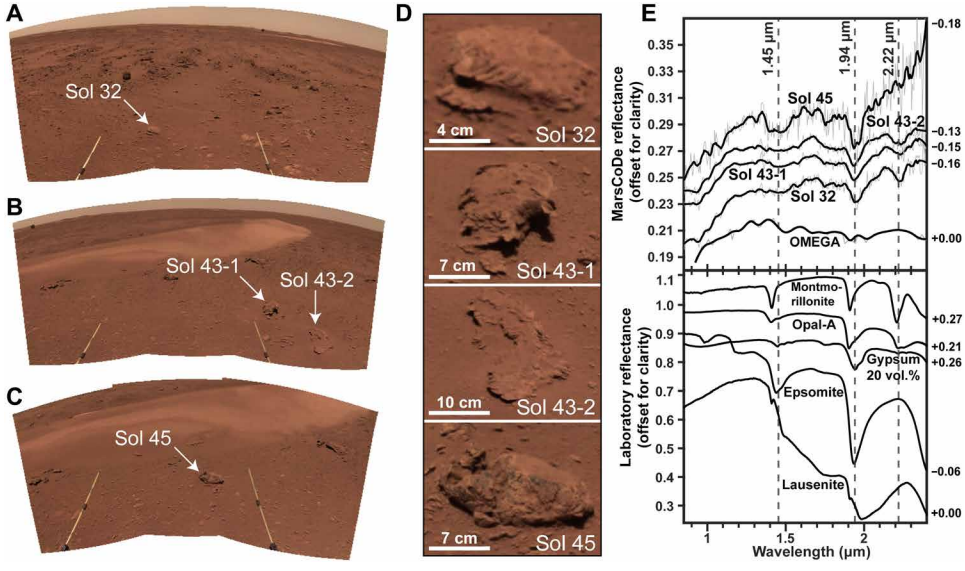

Fig. 3. Spectral observations. The NaTeCam panoramas display the local context for MarSCoDe observations on (**A**) sol 32, (**B**) sol 43, and (**C**) sol 45. The white arrows denote the locations of the rocks targeted for spectral observations. (**D**) Zoomed images for rocks targeted for spectral measurements. (**E**) Comparison between MarSCoDe SWIR spectra with laboratory spectra. The top panel shows the smoothed MarSCoDe spectra (thick solid line) overlays the raw spectra (thin solid line). The signal-to-noise of SWIR data before denoising is around 40 to 55 dB (*24*). The orbital spectrum from OMEGA over the landing area is also plotted for comparison (orbit identification number: ORB0973_5, pixel location: sample 19, line 1296). Note that the small dents in the 1.9- to 2.0-μm region in the OMEGA data are residuals of CO_2 absorptions from the atmospheric correction. Laboratory candidate reflectance spectra are shown in the bottom panel. The IDs for MarSCoDe SWIR and laboratory spectra are tabulated in tables S1 and S2, respectively.

the ground (Fig. 4A and fig. S6). These rock slabs are light-toned, have irregular and rough surfaces, and show significantly different morphology and macrotexture from the dark-toned basalts at this site or pristine basalts at previous landing sites on Mars (*31*, *32*). They are also distinctive from those bright rocks with dark interiors but light-toned rinds. As shown in Fig. 4B, one platy rock slab and its broken fragment show similar texture and morphology as those have examined by Zhurong's MarSCoDe SWIR spectrometer (Fig. 3, A and B). The similar morphology and proximity suggest that the platy rock slabs and those light-toned clasts with fine-layered structures may share a similar origin. The platy rocks are generally resistant to deflation and therefore preserved with a fine-layered structure due to physical weathering.

DISCUSSION

We interpret these bright-toned rocks to be a layer of locally developed duricrust. Unlike the weak and friable thin veneer or crusty clods at previous landing sites for Mars Exploration Rovers and InSight lander [e.g., (*33*, *34*)], these rocks are more akin to the fractured duricrust observed at the Viking Lander 1 site (*35*). The thin and brittle layer of duricrust has been proposed to form by salt cementation via water vapor diffusion from the atmosphere (*35*). In contrast, duricrusts at Zhurong landing site appear to be more resistant to erosion, forming cliffs perched through loose soils in the surroundings, which require a substantial amount of liquid water rather than water vapor. Possible fluvial and lacustrine processes are considered; however, no apparent surface runoff or fluvial channels have been found in the surrounding area. In addition, a puffy, crunchy surface formed by water evaporation and efflorescent salt residuals has not been identified along the traverse. Hydrated sulfates may form through notable acid weathering of dust and sand inside the ice deposit when volcanic aerosols dissolve in the thin films of water to create acidic solutions (*36*); however, this process has difficulty explaining the duricrust features. Therefore, one scenario that we prefer is that the predepositional regolith underwent cementation and lithification during the rising or infiltration of briny groundwater to form the observed platy rocks (Fig. 5). The salt cements (e.g., sulfates or opaline silica) precipitate from the groundwater in the capillary fringe zone, where active evaporation and accumulation can occur (*37*). Episodic fluctuation of the groundwater table may further thicken the indurated section and result in a fine-layered structure. After evaporation, the regolith overlying the duricrust is subject to deflation and erosion, while the duricrusts are resistant to aeolian erosion (*38*). In this scenario, kilometer-scale briny groundwater may have been episodically active and interacting with the colluvium at the landing site. Alternatively, aqueous minerals such as hydrated silica have been observed to be associated with flow features and pitted cones elsewhere in the northern plains (*12*), and the observed mineralogy and duricrust in this work may have some generic link with the pitted cones in the vicinity of the rover (Fig. 1), which requires further investigation by the Tianwen-1 orbiter and Zhurong rover. Last, the type and the nature of the duricrusts (e.g., silcrete, gypcrete, and ferricrete) reported here are now unconstrained. Detailed investigations of the elemental and mineralogical compositions and microtextures of the proposed duricrusts along the rover's traverse may further constrain the origin of these platy rocks and the physicochemical conditions of the relevant liquid water activities during the Amazonian.

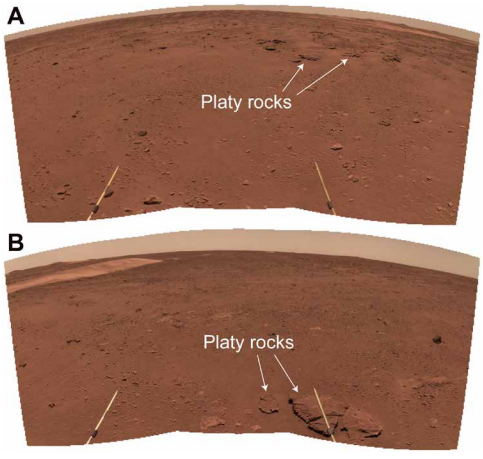

Fig. 4. Observed platy-like rocks along the traverse. (**A**) The NaTeCam mosaic on sol 107 displays continuously distributed platy rocks in perched positions on the surface. (**B**) The NaTeCam mosaic on sol 94 shows the platy rock slab broken in situ on the right and a clastic rock detached from the parent platy rocks nearby. The isolated clast shares similar morphology and texture to those examined by MarSCoDe SWIR spectrometer in Fig. 3.

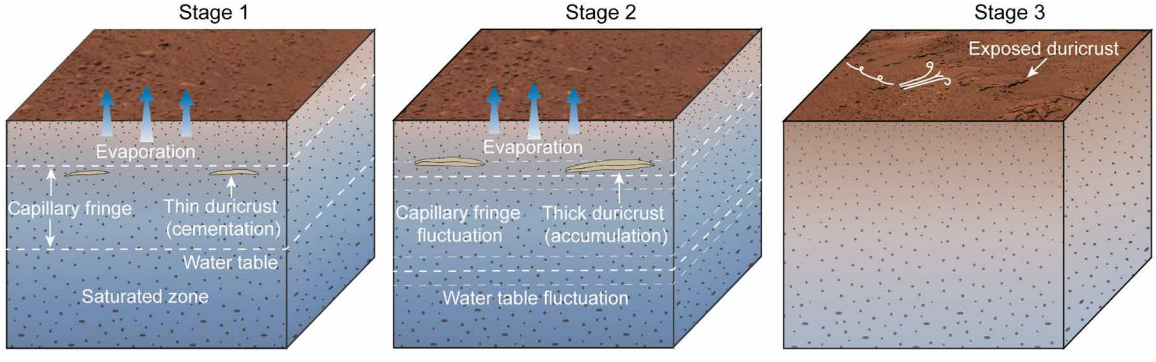

Fig. 5. Schematic model of the duricrust formation process at Zhurong landing site. Stage 1: Evaporation occurs near the groundwater table and in the capillary fringe zone where salt cements (e.g., sulfates or opaline silica) precipitate. The cementation and lithification of predepositional regolith form a thin layer of duricrusts. Stage 2: Episodic fluctuation of the groundwater table further thickens the indurated section to form thick duricrusts with fine-layered structure. Stage 3: The deflation and erosion of the loose sediments exposes the erosion-resistant duricrusts.

The morphology and spatial extent of platy and bright-toned rocks investigated by the Zhurong rover argue for in situ formation and degradation of these rocks in the Amazonian-aged geological unit in southern Utopia Planitia. These observations suggest that aqueous activities may have persisted much longer than previously thought. Periodical climate cycles on Mars driven by obliquity oscillations are expected to result in a latitude-dependent distribution of ground ice over geologic history (*4*, *39*, *40*). Higher obliquities (>45°) could mobilize polar ice and form glaciers and water ice sheets at midlatitudes (*41*) and stabilize ground ice at Zhurong landing site for extended periods of tens of thousand years when the obliquity exceeded 29° to 33° (*42*). The hydrated minerals and widespread salt cementations imply the presence of briny liquid water in the subsurface, which may have been generated by melting the ground ice during temporary climate perturbations (e.g., volcanism and impacts). Specifically, possible dike swarms responsible for landform formation (*20*) or recent volcanism from the Elysium region (*43*) could have been a heat source for maintaining the groundwater system or melting the ice. Alternatively, local transient liquid water under current climate condition may be responsible for local melting of subsurface ground ice, forming indurated duricrust (*44*), in which case the water-rock interaction and the spatial extent would be limited. Determining the mineralogy and spatial extent of the platy rocks in future traverse would provide clues to distinguish different climate conditions for these water activities. Regardless of the potential heat source, the in situ observations manifest recent aqueous activities on Mars, suggesting that the cold and dry late Amazonian epoch may have been episodically punctuated by short-duration climatic warming events that result in melting of ground ice at latitude less than 30°N. The in situ identification of such environments points to a more active Amazonian surface hydrosphere for Mars than previously considered. The Zhurong landing site (and the northern lowlands) may contain a considerable amount of accessible water in the form of hydrated minerals and possibly ground ice for in situ resource utilization for future human Mars exploration.

MATERIALS AND METHODS

In situ SWIR spectral dataset

The MarSCoDe includes a laser-induced breakdown spectrometer, a telescopic microimaging camera, and a SWIR spectrometer (*24*). The SWIR spectrometer is designed to identify the mineralogy of the martian surface with a standoff distance of 1.6 to 7 m. The major detection targets are rocks and other fascinating features in the nominal mission phase (*13*).

The SWIR data have 321 bands with wavelengths ranging from 850 to 2400 nm. The spectral resolution is 3 to 12 nm, and the FOV is 36.5 mrads. The released raw spectra of SWIR have been processed into level 2B (*45*). Specifically, the dark current calibration and absolute radiometric calibration have been conducted. The accuracy of the absolute radiometric calibration is less than 5% (*24*). As shifts in the channel center wavelengths are likely to occur for spectrometer after launch, we performed the spectral drift correction using the pipeline described in (*46*).

Two calibration panels (with reflectance being 99 and 40%, respectively) produced by Labsphere Inc. are installed on the rover. The absolute reflectances of the two calibration panels were measured at Anhui Institute of Optics and Fine Mechanics, Chinese Academy of Sciences. The SWIR spectrometer first collected the radiance of 99 and 40% spectralon before measuring the target. All the SWIR spectra used in this work are tabulated in table S1. The reflectance of SWIR data is lastly obtained with Eq. 1

$$Ref_{\mathrm{tar}} = \frac{Rad_{\mathrm{tar}}}{Rad_{\mathrm{cal}}} \times Ref_{\mathrm{cal}} \quad (1)$$

where Rad_{tar} and Rad_{cal} denote the radiance data of the observed target and calibration panel, respectively. Ref_{tar} and Ref_{cal} represent the reflectance of the target and calibration panel, respectively. In practice, the 99% reflectance spectralon is preferred unless overexposed.

The NaTeCam dataset

The NaTeCams are binocular stereo cameras mounted on the Mars rover mast about 1.2 m above the surface. They are designed to provide support for the guidance, navigation, and control of the rover (*25*). The NaTeCam investigates the terrains around the rover and determines the locations and shapes of potential targets.

The NaTeCam is a color imaging system using a complementary metal oxide semiconductor–active pixel sensor. The depth of field of each camera is from 0.5 m to infinity, and the best focus is 1 m (*25*). The camera's FOV is 46.5° × 46.5°. The effective pixel number is 2048 × 2048, and the pixel resolution is 5.5 μm.

In addition to the dark current removal and relative radiometric calibration to generate the data of levels 2A and 2B, the NaTeCam image from Bayer format was further converted to an RGB-per-pixel format in level 2C (*45*). All the NaTeCam images used in this work are tabulated in table S1.

Spectral analysis

In addition to visual inspection, we performed detailed spectral analysis on the MarSCoDe SWIR spectra to verify the potential spectral matches. We compared the MarSCoDe SWIR spectra to laboratory spectra of hydrated silica and sulfates (fig. S5 and table S2). We also plotted the spectra of the mixtures of gypsum and Mars Global Simulant (*47*) for comparison. The MarSCoDe SWIR spectra are first denoised by the Savitzky-Golay algorithm (*48*) with 31 points and a second polynomial order. As shown in fig. S5, the 1.9-μm band center of the SWIR spectra ranges from 1.93 to 1.95 μm, more consistent with sulfates. The 2.2-μm band center of the SWIR spectra varies between 2.20 and 2.26 μm. Such variations suggest the signal is not strong enough for a definitive interpretation. If these variations were native to the target material, then a mixed origin of multiple mineral species with 2.2-μm absorption is possible.

The FOV of the MarSCoDe SWIR spectrometer is in the same order as the size of the rocks measured. As a result, the spectral data include a mixture of light scattered from the rock surface, dust cover, and martian soil. The relevant contribution from each part of the surface cannot be directly quantified with the data available. Because the orbital data do not show the same absorption features (Fig. 2E), these spectral detections most likely correspond to the rock composition or materials locally derived from the light-toned rocks rather than a more globally distributed dust component. Future detection using MarSCoDe SWIR spectrometer with multiple observations of the same target with varying amounts of mixing can be used to determine the contribution of the various components at Zhurong's landing site.

SUPPLEMENTARY MATERIALS

Supplementary material for this article is available at https://science.org/doi/10.1126/sciadv.abn8555

REFERENCES AND NOTES

1. R. M. Haberle, R. T. Clancy, F. Forget, M. D. Smith, R. W. Zurek, *The Atmosphere and Climate of Mars* (Cambridge Univ. Press, 2017).
2. J.-P. Bibring, Y. Langevin, J. F. Mustard, F. Poulet, R. Arvidson, A. Gendrin, B. Gondet, N. Mangold, P. Pinet, F. Forget, M. Berthé, J.-P. Bibring, A. Gendrin, C. Gomez, B. Gondet, D. Jouglet, F. Poulet, A. Soufflot, M. Vincendon, M. Combes, P. Drossart, T. Encrenaz, T. Fouchet, R. Merchiorri, G. Belluci, F. Altieri, V. Formisano, F. Capaccioni, P. Cerroni, A. Coradini, S. Fonti, O. Korablev, V. Kottsov, N. Ignatiev, V. Moroz, D. Titov, L. Zasova, D. Loiseau, N. Mangold, P. Pinet, S. Douté, B. Schmitt, C. Sotin, E. Hauber, H. Hoffmann, R. Jaumann, U. Keller, R. Arvidson, J. F. Mustard, T. Duxbury, F. Forget, G. Neukum, Global mineralogical and aqueous mars history derived from OMEGA/Mars Express data. *Science* **312**, 400–404 (2006).
3. A. M. Bramson, S. Byrne, N. E. Putzig, S. Sutton, J. J. Plaut, T. C. Brothers, J. W. Holt, Widespread excess ice in Arcadia Planitia, Mars. *Geophys. Res. Lett.* **42**, 6566–6574 (2015).
4. J. W. Head, J. F. Mustard, M. A. Kreslavsky, R. E. Milliken, D. R. Marchant, Recent ice ages on Mars. *Nature* **426**, 797–802 (2003).
5. J. F. Mustard, C. D. Cooper, M. K. Rifkin, Evidence for recent climate change on Mars from the identification of youthful near-surface ground ice. *Nature* **412**, 411–414 (2001).
6. D. E. J. Hobley, A. D. Howard, J. M. Moore, Fresh shallow valleys in the Martian midlatitudes as features formed by meltwater flow beneath ice: Fresh shallow valleys formed beneath ice. *J. Geophys. Res. Planets* **119**, 128–153 (2014).
7. S. Adeli, E. Hauber, M. Kleinhans, L. Le Deit, T. Platz, P. Fawdon, R. Jaumann, Amazonian-aged fluvial system and associated ice-related features in Terra Cimmeria, Mars. *Icarus* **277**, 286–299 (2016).
8. L. Pan, B. L. Ehlmann, Aqueous processes from diverse hydrous minerals in the vicinity of amazonian-aged Iyot crater. *J. Geophys. Res. Planets* **123**, 1618–1648 (2018).
9. K. L. Tanaka, Resurfacing history of the northern plains of Mars based on geologic mapping of Mars Global Surveyor data. *J. Geophys. Res.* **108**, 8043 (2003).
10. J. Carter, F. Poulet, J.-P. Bibring, S. Murchie, Detection of hydrated silicates in crustal outcrops in the northern plains of Mars. *Science* **328**, 1682–1686 (2010).
11. L. Pan, B. L. Ehlmann, J. Carter, C. M. Ernst, The stratigraphy and history of Mars' northern lowlands through mineralogy of impact craters: A comprehensive survey: Stratigraphy of Mars' northern lowlands. *J. Geophys. Res. Planets* **122**, 1824–1854 (2017).
12. J. Carter, F. Poulet, J.-P. Bibring, N. Mangold, S. Murchie, Hydrous minerals on Mars as seen by the CRISM and OMEGA imaging spectrometers: Updated global view. *J. Geophys. Res. Planets* **118**, 831–858 (2013).
13. J. Liu, C. Li, R. Zhang, W. Rao, X. Cui, Y. Geng, Y. Jia, H. Huang, X. Ren, W. Yan, X. Zeng, W. Wen, X. Wang, X. Gao, Q. Fu, Y. Zhu, J. Dong, H. Li, X. Wang, W. Zuo, Y. Su, D. Kong, H. Zhang, Geomorphic contexts and science focus of the Zhurong landing site on Mars. *Nat Astron.* 1–7 (2021).
14. G. E. McGill, Buried topography of Utopia, Mars: Persistence of a giant impact depression. *J. Geophys. Res.* **94**, 2753–2759 (1989).
15. K. L. Tanaka, J. A. Skinner, T. M. Hare, Geologic Map of the Northern Plains of Mars, *U.S. Geological Survey Scientific Investigations Map 2888* (U.S. Geological Survey, 2005).
16. M. A. Ivanov, H. Hiesinger, G. Erkeling, D. Reiss, Mud volcanism and morphology of impact craters in Utopia Planitia on Mars: Evidence for the ancient ocean. *Icarus* **228**, 121–140 (2014).
17. B. Wu, J. Dong, Y. Wang, Z. Li, Z. Chen, W. C. Liu, J. Zhu, L. Chen, Y. Li, W. Rao, Characterization of the candidate landing region for Tianwen-1—China's first mission to Mars. *Earth Space Sci.* **8**, (2021).
18. X. Wu, Y. Liu, C. Zhang, Y. Wu, F. Zhang, J. Du, Z. Liu, Y. Xing, R. Xu, Z. He, Y. Lin, Y. Zou, Geological characteristics of China's Tianwen-1 landing site at Utopia Planitia, Mars. *Icarus* **370**, 114657 (2021).
19. M. M. Mills, A. S. McEwen, C. H. Okubo, A preliminary regional geomorphologic map in Utopia Planitia of the Tianwen-1 Zhurong landing region. *Geophys. Res. Lett.* **48**, e2021GL094629 (2021).
20. B. Ye, Y. Qian, L. Xiao, J. R. Michalski, Y. Li, B. Wu, L. Qiao, Geomorphologic exploration targets at the Zhurong landing site in the southern Utopia Planitia of Mars. *Earth Planet. Sci. Lett.* **576**, 117199 (2021).
21. J. Zhao, Z. Xiao, J. Huang, J. W. Head, J. Wang, Y. Shi, B. Wu, L. Wang, Geological characteristics and targets of high scientific interest in the Zhurong landing region on Mars. *Geophys. Res. Lett.* **48**, e2021GL094903 (2021).
22. W. X. Wan, C. Wang, C. L. Li, Y. Wei, China's first mission to Mars. *Nat. Astron.* **4**, 721–721 (2020).
23. Y. Zou, Y. Zhu, Y. Bai, L. Wang, Y. Jia, W. Shen, Y. Fan, Y. Liu, C. Wang, A. Zhang, G. Yu, J. Dong, R. Shu, Z. He, T. Zhang, A. Du, M. Fan, J. Yang, B. Zhou, Y. Wang, Y. Peng, Scientific objectives and payloads of Tianwen-1, China's first Mars exploration mission. *Adv. Space Res.* **67**, 812–823 (2021).
24. W. Xu, X. Liu, Z. Yan, L. Li, Z. Zhang, Y. Kuang, H. Jiang, H. Yu, F. Yang, C. Liu, T. Wang, C. Li, Y. Jin, J. Shen, B. Wang, W. Wan, J. Chen, S. Ni, Y. Ruan, R. Xu, C. Zhang, Z. Yuan, X. Wan, Y. Yang, Z. Li, Y. Shen, D. Liu, B. Wang, R. Yuan, T. Bao, R. Shu, The MarSCoDe instrument suite on the mars rover of China's Tianwen-1 mission. *Space Sci. Rev.* **217**, 64 (2021).
25. X. Liang, W. Chen, Z. Cao, F. Wu, W. Lyu, Y. Song, D. Li, C. Yu, L. Zhang, L. Wang, The navigation and terrain cameras on the Tianwen-1 Mars rover. *Space Sci. Rev.* **217**, 37 (2021).
26. M. A. Presley, P. R. Christensen, Thermal conductivity measurements of particulate materials 1. A review. *J. Geophys. Res.* **102**, 6535–6549 (1997).
27. R. E. Milliken, G. A. Swayze, R. E. Arvidson, J. L. Bishop, R. N. Clark, B. L. Ehlmann, R. O. Green, J. P. Grotzinger, R. V. Morris, S. L. Murchie, J. F. Mustard, C. Weitz, Opaline silica in young deposits on Mars. *Geology* **36**, 847–850 (2008).
28. Y. Langevin, F. Poulet, J.-P. Bibring, B. Gondet, Sulfates in the North polar region of Mars detected by OMEGA/Mars express. *Science* **307**, 1584–1586 (2005).
29. X. Wu, J. F. Mustard, J. D. Tarnas, X. Zhang, E. Das, Y. Liu, Imaging Mars analog minerals' reflectance spectra and testing mineral detection algorithms. *Icarus* **369**, 114644 (2021).
30. M. Pineau, L. Le Deit, B. Chauviré, J. Carter, B. Rondeau, N. Mangold, Toward the geological significance of hydrated silica detected by near infrared spectroscopy on Mars based on terrestrial reference samples. *Icarus* **347**, 113706 (2020).
31. T. A. Mutch, R. E. Arvidson, A. B. Binder, E. A. Guinness, E. C. Morris, The geology of the Viking Lander 2 site. *J. Geophys. Res.* **82**, 4452–4467 (1977).
32. S. W. Squyres, R. E. Arvidson, J. F. Bell, J. Brückner, N. A. Cabrol, W. Calvin, M. H. Carr, P. R. Christensen, B. C. Clark, L. Crumpler, D. J. D. Marais, C. d'Uston, T. Economou, J. Farmer, W. Farrand, W. Folkner, M. Golombek, S. Gorevan, J. A. Grant, R. Greeley, J. Grotzinger, L. Haskin, K. E. Herkenhoff, S. Hviid, J. Johnson, G. Klingelhöfer, A. Knoll, G. Landis, M. Lemmon, R. Li, M. B. Madsen, M. C. Malin, S. M. McLennan, H. Y. McSween, D. W. Ming, J. Moersch, R. V. Morris, T. Parker, J. W. Rice, L. Richter, R. Rieder, M. Sims, M. Smith, P. Smith, L. A. Soderblom, R. Sullivan, H. Wänke, T. Wdowiak, M. Wolff, A. Yen, The spirit rover's athena science investigation at gusev crater, Mars. *Science* **305**, 794–799 (2004).
33. J. A. Hurowitz, S. M. McLennan, N. J. Tosca, R. E. Arvidson, J. R. Michalski, D. W. Ming, C. Schröder, S. W. Squyres, In situ and experimental evidence for acidic weathering of rocks and soils on Mars. *J. Geophys. Res. Planets* **111**, E02S19 (2006).
34. M. Golombek, N. H. Warner, J. A. Grant, E. Hauber, V. Ansan, C. M. Weitz, N. Williams, C. Charalambous, S. A. Wilson, A. DeMott, M. Kopp, H. Lethcoe-Wilson, L. Berger, R. Hausmann, E. Marteau, C. Vrettos, A. Trussell, W. Folkner, S. Le Maistre, N. Mueller, M. Grott, T. Spohn, S. Piqueux, E. Millour, F. Forget, I. Daubar, N. Murdoch, P. Lognonné, C. Perrin, S. Rodriguez, W. T. Pike, T. Parker, J. Maki, H. Abarca, R. Deen, J. Hall, P. Andres, N. Ruoff, F. Calef, S. Smrekar, M. M. Baker, M. Banks, A. Spiga, D. Banfield, J. Garvin, C. E. Newman, W. B. Banerdt, Geology of the InSight landing site on Mars. *Nat. Commun.* **11**, 1014 (2020).
35. C. D. Cooper, J. F. Mustard, Spectroscopy of loose and cemented sulfate-bearing soils: Implications for duricrust on Mars. *Icarus* **158**, 42–55 (2002).
36. P. B. Niles, J. Michalski, Meridiani Planum sediments on Mars formed through weathering in massive ice deposits. *Nat. Geosci.* **2**, 215–220 (2009).
37. J. K. Warren, Depositional chemistry and hydrology, in *Evaporites* (Springer, 2016), pp. 85–205.
38. M. Williams, Desert soils, paleosols and duricrusts, in *Climate Change in Deserts: Past, Present and Future* (Cambridge Univ. Press, 2014), pp. 258–282.
39. W. R. Ward, Climatic variations on Mars: 1. Astronomical theory of insolation. *J. Geophys. Res.* **79**, 3375–3386 (1974).
40. J. Laskar, A. C. M. Correia, M. Gastineau, F. Joutel, B. Levrard, P. Robutel, Long term evolution and chaotic diffusion of the insolation quantities of Mars. *Icarus* **170**, 343–364 (2004).
41. F. Forget, R. M. Haberle, F. Montmessin, B. Levrard, J. W. Head, Formation of glaciers on Mars by atmospheric precipitation at high obliquity. *Science* **311**, 368–371 (2006).
42. M. T. Mellon, H. G. Sizemore, The history of ground ice at Jezero crater Mars and other past, present, and future landing sites. *Icarus* **371**, 114667 (2022).
43. D. G. Horvath, P. Moitra, C. W. Hamilton, R. A. Craddock, J. C. Andrews-Hanna, Evidence for geologically recent explosive volcanism in Elysium Planitia, Mars. *Icarus* **365**, 114499 (2021).
44. R. M. Haberle, C. P. McKay, J. Schaeffer, N. A. Cabrol, E. A. Grin, A. P. Zent, R. Quinn, On the possibility of liquid water on present-day Mars. *J. Geophys. Res. Planets* **106**, 23317–23326 (2001).
45. X. Tan, J. Liu, X. Zhang, W. Yan, W. Chen, X. Ren, W. Zuo, C. Li, Design and validation of the scientific data products for China's Tianwen-1 mission. *Space Sci. Rev.* **217**, 69 (2021).
46. T. Wang, G. Yan, H. Ren, X. Mu, Improved methods for spectral calibration of on-orbit imaging spectrometers. *IEEE Trans. Geosci. Remote Sens.* **48**, 3924–3931 (2010).

47. J. D. Tarnas, J. F. Mustard, X. Wu, E. Das, K. M. Cannon, C. B. Hundal, A. C. Pascuzzo, J. R. Kellner, M. Parente, Successes and challenges of factor analysis/target transformation application to visible-to-near-infrared hyperspectral data. *Icarus* **365**, 114402 (2021).
48. A. Savitzky, M. J. Golay, Smoothing and differentiation of data by simplified least squares procedures. *Anal. Chem.* **36**, 1627–1639 (1964).
49. D. E. Smith, M. T. Zuber, H. V. Frey, J. B. Garvin, J. W. Head, D. O. Muhleman, G. H. Pettengill, R. J. Phillips, S. C. Solomon, H. J. Zwally, W. B. Banerdt, T. C. Duxbury, M. P. Golombek, F. G. Lemoine, G. A. Neumann, D. D. Rowlands, O. Aharonson, P. G. Ford, A. B. Ivanov, C. L. Johnson, P. J. McGovern, J. B. Abshire, R. S. Afzal, X. Sun, Mars Orbiter Laser Altimeter: Experiment summary after the first year of global mapping of Mars. *J. Geophys. Res. Planets* **106**, 23689–23722 (2001).
50. Q. Meng, D. Wang, X. Wang, W. Li, X. Yang, D. Yan, Y. Li, Z. Cao, Q. Ji, T. Sun, W. Yan, K. Wang, X. Li, J. Huang, Z. Wang, W. Zhao, Y. Wang, Y. He, X. Hao, W. Liu, B. Zhang, P. Zhou, Y. Li, H. Zhao, L. Lu, H. Guan, D. Zhou, F. Wu, F. Zhang, S. Zhu, J. Dong, High resolution imaging camera (HiRIC) on China's first Mars exploration Tianwen-1 mission. *Space Sci. Rev.* **217**, 42 (2021).
51. M. C. Malin, J. F. Bell III, B. A. Cantor, M. A. Caplinger, W. M. Calvin, R. T. Clancy, K. S. Edgett, L. Edwards, R. M. Haberle, P. B. James, S. W. Lee, M. A. Ravine, P. C. Thomas, M. J. Wolff, Context camera investigation on board the Mars Reconnaissance Orbiter. *J. Geophys. Res. Planets* **112**, E05S04 (2007).
52. V. Z. Sun, "Clays and opals on Mars: Implications for water-rock interactions through time," thesis, Brown University, Providence, RI (2017).
53. C. M. Pieters, Strength of mineral absorption features in the transmitted component of near-infrared reflected light: First results from RELAB. *J. Geophys. Res.* **88**, 9534–9544 (1983).
54. R. N. Clark, G. A. Swayze, R. A. Wise, K. E. Livo, T. M. Hoefen, R. F. Kokaly, S. J. Sutley, U.S. Geological Survey, USGS Digital Spectral Library 06 (USGS, 2007); http://speclab.cr.usgs.gov/spectral.lib06.

Acknowledgments: We thank the Tianwen-1 engineering team for such a successful mission, payload team for mission operations, and China National Space Administration (CNSA) for providing the Tianwen-1 scientific data that made this study possible. This dataset is processed and produced by Ground Research and Application System (GRAS) of China's Lunar and Planetary Exploration Program, provided by CNSA (http://moon.bao.ac.cn). We thank three anonymous reviewers for insightful comments. **Funding:** This work was supported by the Key Research Program of the Chinese Academy of Sciences (ZDBS-SSW-TLC001); the Strategic Priority Research Program of CAS (XDB 41000000); National Natural Science Foundation of China (42072337); the preresearch project on Civil Aerospace Technologies funded by CNSA (no. D020102 and no. D020101); Pandeng Program of National Space Science Center, Chinese Academy of Sciences; and Carlsberg Foundation, Denmark (grant CF18_1105).
Author contributions: Design and lead of this research: Y.L. Conceptualization: Y.L., Y.Z., and L.P. Data processing and calibration: Y.L. and X.W. Data interpretation: Y.L., Y.Z., and L.P. Methodology: Y.L., X.W., J.L., Z.Z., X.Z., C.Z., Y.W., and W.W. Visualization: Y.L., X.W., J.L., Z.Z., X.Z., C.Z., Y.W., and W.W. Supervision: Y.L., C.W., and Y.Z. Funding acquisition: Y.L. Writing—original draft: Y.L., Y.Z., L.P., and X.W. Writing—review and editing: All the authors. **Competing interests:** The authors declare that they have no competing interests. **Data and materials availability:** All data needed to evaluate the conclusions in the paper are present in the paper and/or the Supplementary Materials. The data reported in this work are available at the Lunar and Planetary Data Release System (https://moon.bao.ac.cn/web/enmanager/home). Path to access the data: Home Page>Scientific Data>Mars.

Submitted 23 December 2021
Accepted 5 April 2022
Published 11 May 2022
10.1126/sciadv.abn8555

ScienceAdvances

Zhurong reveals recent aqueous activities in Utopia Planitia, Mars

Yang Liu, Xing Wu, Yu-Yan Sara Zhao, Lu Pan, Chi Wang, Jia Liu, Zhenxing Zhao, Xiang Zhou, Chaolin Zhang, Yuchun Wu, Wenhui Wan, and Yongliao Zou

Sci. Adv., **8** (19), eabn8555.
DOI: 10.1126/sciadv.abn8555